# Numerical Investigation of Thermal Stratification and Numerical Diffusion in a Large-scale Water Pits Heat Storage

**Meng Gao, Jianhua Fan and Simon Furbo**

Department of Civil and Mechanical Engineering, Technical University of Denmark, Kgs. Lyngby, Denmark

**Abstract**

Large scale water pit heat storage (PTES) is a key component to increase the efficiency of solar thermal utilization. Based on the 1535-1301 model, this paper presents a two-dimensional simulation of the annual thermal performance of PTES using TRNSYS. This model encrypts the soil grid according to the water pit layers to improve the accuracy of heat loss calculation. The accuracy of the model is verified by comparing it with measured data from a solar plant in Dronninglund, Denmark. The results show that the average difference between the model and the measured data is approximately 2.5%. In addition, the temperature prediction error and numerical diffusion of each layer become smaller as the nodes number increases. The stratification coefficient averages about 200 for summer charging and decrease to 100 for winter discharging, Mix number is 0.7 at charge and 0.35 at minimum, indicating that stratification is more pronounced in summer and mixing is higher in winter. The parametric coupling study found that the nodes number and the time step are more accurate when they are negatively correlated, i.e., fewer nodes are paired with longer time steps. Adiabatic admixture decreases the Mix number prediction accuracy but increases the stratification coefficient one.

*Keywords: Water pit heat storage, Numerical investigation, Thermal stratification, large-scale, numerical diffusion*

## 1. Introduction

Reducing the utilization of fossil resources and carbon emission is very important for sustainable development around the world. Renewable energy, such as solar energy, is one of the main ways to solve this problem. As known to all, thermal storage technology is a key measure to solve the problem of low density, discontinuous fluctuation and unreliability of renewable energy, which can realize effective regulation of heat. Especially, seasonal thermal storage is significant in the large-scale district application of renewable energy (Vega, 2010).

Different STES technologies and applications have been extensively studied. The STES are normally categorized into four types: tank thermal energy storage (TTES), pit thermal energy storage (PTES), borehole thermal energy storage (BTES), and aquifer thermal energy storage (ATES) (Bauer, 2010). The best solution should be determined based on technical-economic assessment considering storage capacity, efficiency, requirements on regional conditions, building cost, etc. Originated from landfill technology, PTES has the advantages of high heat capacity, low construction investment, good corrosion protection and effective heat exchange. In recent years, many attempts of larger PTES have been carried out in Europe. More than 10 large-scale PTESs have been put into operation in Denmark (Bott, 2019).

Denmark is currently the leading country in the application of PTES. The first large PTES with a volume of 500 $m^3$ was built at the Technical University of Denmark and was investigated intensively (Heller, 1997). In the last decade, 75% of PTES construction projects have been built in Denmark (Bratseth, 2021). The integration of PTES on such a large scale is difficult to plan and implement because technical and economic differences pose different challenges for each country (Dahash, 2019). The commercialization of PTES is expected to accelerate in the coming years. However, large-scale PTES testing is difficult due to high experimental costs. Therefore, modeling and design optimization of PTES play a key role in ensuring feasibility.

TRNSYS performs well as a software for system simulation in modeling thermal storage of different types. However, the existing literature studies focus more on the system simulation including the selection and operation strategies of thermal storage. Few studies on thermal storage and especially PTES models have been especially validated by measurements. The current TRNSYS models are simplified to a vertical one-dimensional model of the water pit to reduce computational resources (Pan, 2022). The reason is that PTES shows a significant thermal stratification along


doi:10.18086/eurosun.2022.13.10 Available at http://proceedings.ises.org

the depth, while the horizontal temperature gradient is not prominent enough to be negligible. However, this simplification leads to some additional problems, i.e., numerical diffusion due to grid size and time step, and inverse mixing due to temperature differences in water delivery (Xiang, 2022). If these problems are not solved will result in large deviations in the calculation results and affect the accuracy of models.

In this paper, a model of PTES (Type 1535-1301) from TRNSYS containing 1D water pit and 2D soil is used as a research object. The measured data of 60,000 $m^3$ of PTES in Dronninglund, Denmark, in 2017 are utilized as input parameters and validation data. The stratification coefficient and Mix number are taken as an indicator to evaluate the stratification effect during the energy charging and discharging period. The coupling effects of layer number, time step and mixing revisions on the computational accuracy are investigated. The quantitative equation of the deviation value versus the simulation parameters is obtained by comparing the measured data. Thus, the discrete differences due to the simplification of the computational domain are corrected.

## 2. Methodology

### 2.1. The structure and principle of PTES

The geometry of the PTES at the Dronninglund SDH plant is an inverted truncated pyramid with a slope angle of 26.6°, as shown in Fig. 1. The lengths of the top and bottom edges are 90 m and 26 m, respectively. Three diffusers are installed at the top, middle and bottom of the water pit, switching as inlet or outlet according to the system's operating strategy. Disc-shaped stratifiers located above and below the diffusers greatly reduce turbulent mixing and maintain stable thermal stratification. During rainy days, nights or when heat demand is high, hot water is delivered from the top and cold water is fed to the bottom. At this time, the internal energy of PTES is reduced in what is called the discharge period. In sunny days, hot water is imported at the top and cold water is exported from the bottom. The increase of PTES energy at this moment is called the charge period.

Since the PTES is buried monolithically with only a 2.5 mm HDPE liner and a 2 mm geotextile layer on its sides and bottom, there is no additional insulation. Because the surrounding soil serves both as insulation and as a medium for thermal energy storage. Covering the top of the water pit storage with insulation is an effective way to reduce heat loss. In addition, multiple sets of drainage pipes are installed between the insulation and the waterproofing layer to prevent rainwater infiltration.

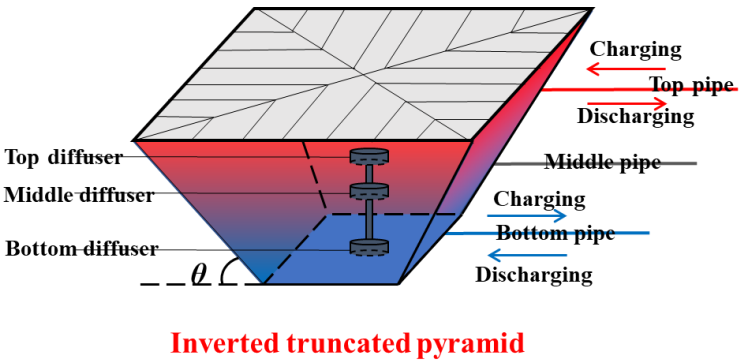


**Fig. 1: The structure of water pit heat storage**

### 2.2. The grid scheme of PTES

A PTES model written in FORTRAN is developed on TRNSYS, named type 1535-1301. The type 1535 is a one-dimensional water pit model including the heat exchanger in the interior. Because PTES has a significant temperature gradient only in the depth direction. The type 1301 is a two-dimensional surrounding soil model including the insulation layer above. The soil temperature varies only in one horizontal direction. The geometry of both types is simplified to central-symmetric inverted cylindrical coordinates with only radius-direction and axial-direction. Fig. 2 shows the mesh of the simplified PTES model. Encryption above and below the baseline of the puddle meshing interface. This gridding allows for more accurate heat transfer simulations at temperature stratification intersections. In addition, the grid near the PTES is refined, while the grid near the bottom soil boundary is coarsened.

In addition, some assumptions are made for the heat transfer calculations. Only half of the water pit is modeled with the left boundary as the axis. The convective coefficient between the water pit and the wall is set to a constant value. Only the thermal conductivity is available in the soil fraction due to the neglect of the effect of moisture and

groundwater flow.

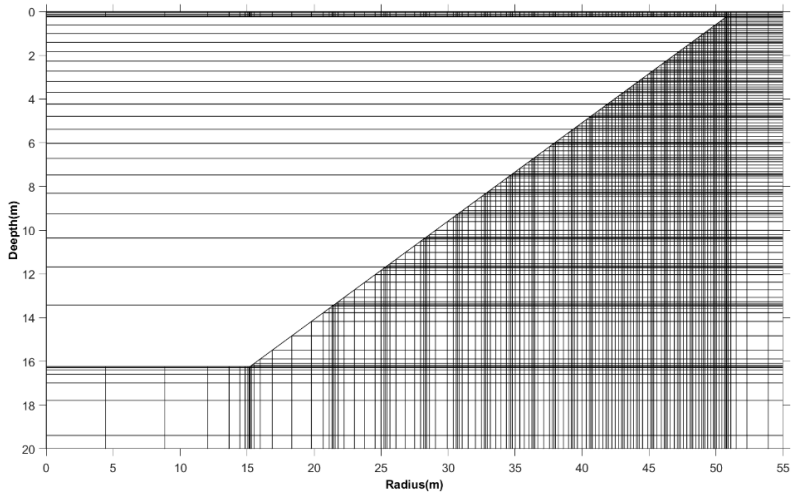


**Fig. 2: The Mesh of Type 1535-1301 model**

2.3. Mathematical description

The water pit node energy is a one-dimensional thermal conductivity calculation (Song, 2003). The explicit central differential form of the one-dimensional thermal conductivity equation is shown in Eq. (1), where the left part of the equation is the instantaneous energy change of the node, and the right part of the equation is the imported energy:

$$V_j C_p \rho_w \frac{\partial T_j}{\partial \tau} = \left[\frac{\lambda_w (r_j - r_{j+1})^2}{(z_{j+1} - z_j)} + m_j C_p + m_{mix,j} C_p\right](T_{j+1} - T_j) + \left(\frac{1}{h_w} + \frac{\delta_{\mathrm{HDPE}}}{\lambda_{\mathrm{HDPE}}} + \frac{\delta_{\mathrm{geo}}}{\lambda_{\mathrm{geo}}}\right)^{-1} A_{side,j}(T_{side,j} - T_j) + V_{in}\rho_w C_p (T_{in} - T_j) + Q_j \quad \text{(eq. 1)}$$

where $Q_j$ denotes the additional energy input or output. At water pit of $j$ = 1 and $j$ = n (top and bottom nodes, respectively), $Q_j$ satisfies the following formula:

$$Q_j = \begin{cases} U_{top} A_1 (T_{top} - T_1), & j = 1 \\ U_{bot} A_n (T_{bot} - T_n), & j = n \end{cases} \quad \text{(eq. 2)}$$

The soil and insulation are two-dimensional grids and therefore follow a two-dimensional heat transfer calculation as shown in Eq. (3). The partial differential equation uses the central difference method with *i,k* representing the radial and vertical nodes.:

$$V_{i,k} c\rho \frac{\partial T_{i,k}}{\partial \tau} = \frac{2 \cdot \lambda_s \cdot A_{i,k+1}}{z_{k+1} - z_k}(T_{i,k+1} - T_{i,k}) + \frac{2 \cdot \lambda_s \cdot A_{i,k-1}}{z_k - z_{k-1}}(T_{i,k-1} - T_{i,k}) + \frac{(z_{k+1} - z_k) \cdot \lambda_s}{2 \ln\left(\frac{r_{i+1}}{r_i}\right)}(T_{i+1,k} - T_{i,k}) + \frac{(z_k - z_{k-1}) \cdot \lambda_s}{2 \ln\left(\frac{r_i}{r_{i-1}}\right)}(T_{i-1,k} - T_{i,k}) + Q_{i,k} \quad \text{(eq. 3)}$$

where $Q_{i,k}$ denotes the boundary heat exchange and satisfies the following formula:

$$Q_{i,k} = \begin{cases} h_{am} A_{i,1}(T_{am} - T_{i,1}), & k = 1 \\ \frac{(z_k - z_{k-1}) \cdot \lambda_s}{\ln\left(\frac{r_{far}}{r_R}\right)} A_{R,k}(T_{far} - T_{R,k}), & i = R, k = (1, Z) \\ \frac{2 \cdot \lambda_s \cdot A_{i,k}}{z_Z - z_{Z-1}} A_{i,NZ}(T_{deep} - T_{i,NZ}), & i = (1, R), k = Z \\ U_{bot} A_{i,Nz}(T_{bot} - T_{i,Nz}), & i = (1, Nr), k = Nz \\ U_{side} A_{i,k}(T_{side,i,k} - T_{i,k}), & i = (Nr, NR), k = (NZ, Nz) \end{cases} \quad \text{(eq. 4)}$$

The average water pit temperature is obtained by volume averaging of all node temperatures, as shown in Eq. (5):

$$\bar{T} = \frac{\sum_{j=1}^{N} T_j V_j}{V_t} \quad \text{(eq. 5)}$$

2.4. Thermal stratification evaluations

Thermal stratification plays a crucial role in assessing the thermal performance of PTES. The optimal thermal stratification is the ideal plug flow, where the tank is divided into a high-temperature upper layer and a low-

temperature lower layer. The ideal thermal stratification allows for the lowest PTES mixing losses and the most stable heat extraction. The higher temperature difference between the top and bottom, the more efficient water-water heat pump as an auxiliary energy source. Furthermore, the lower return water temperature, the heat exchanger efficiency and collector efficiency will be increased. Consequently, even active cooling of the return water is required to obtain better stratification (Pinel, 2011). Mixing number and stratification coefficient are widely used to characterize the thermal stratification in heat storage.

The Eq. (6)-(9) calculate the mixing number by comparing the energy moments (Davidson, 1994), where $M_c$ represents the energy moments obtained from experiments and simulations. When calculating the energy moment $M_{mix}$ of the hybrid accumulator, the temperature of all layers is the same (Haller, 2009). The energy moment for complete stratification is represented by $M_{str}$, as shown in Eq. (8). Where the high and low temperature zone temperatures $T_{hot}$ and $T_{cold}$ are expressed as the highest and lowest inlet temperatures during the test, respectively:

$$M_c = \sum_{j=1}^{N} H_j \, \rho_w V_j C_p \cdot T_j \qquad \text{(eq. 6)}$$

$$M_{mix} = \sum_{j=1}^{N} H_j \, \rho_w V_j C_p \cdot \frac{Q_{sto}}{\rho_w \cdot C_p \cdot V_t} \qquad \text{(eq. 7)}$$

$$M_{str} = \sum_{j=1}^{N_{thermo}} \rho_w \, C_p V_j H_j \cdot T_{hot} + \sum_{j=N_{thermo}}^{N} \rho_w \, C_p V_j H_j \cdot T_{cold} \qquad \text{(eq. 8)}$$

$$MIX = \frac{(M_{str} - M_c)}{(M_{str} - M_{mix})} \qquad \text{(eq. 9)}$$

In addition, the stratification coefficient of equation (10) can also evaluate the thermal stratification effect. The stratification coefficient is more focused on the temperature level than the energy moment (Fernandez, 2007).

$$ST = \frac{\sum_j^N m_j (T_j - \bar{T})^2}{m_t} \qquad \text{(eq. 10)}$$

2.5. Model accuracy analysis

Model 1535-1301 is a pure thermal conductivity model, so discrete uncertainties can be ignored. The simplification of this model may lead to the following inaccurate results. The inlet and outlet values are considered as source terms of the equation and do not consider the thermal processes of the pipe. Changes in water content do not affect the thermal properties of the soil and may lead to an underestimation of heat losses. Constant convection coefficients lead to reduced accuracy in periods of high temperature fluctuations.

By comparing the calculated and measured parameters, the root mean square deviation (RMSD) was used, as shown in eq. (11).

$$RMSD = \sqrt{\frac{1}{N} \sum_{i=1}^{N} \left( P_{sim,i} - P_{mea,i} \right)^2} \qquad \text{(eq. 11)}$$

where, $N$ presents the number of values in whole simulation period. $P_{sim,i}$ and $P_{mea,i}$ are respectively the calculated and the measured parameters every 10 mins.

The coefficient of determination $R^2$ is used to measure the accuracy of the model. This coefficient is a quantitative measure of the degree of variance in the data. Thus, it is possible to see how much of the variance in the data is captured (or predicted) by the modelled data. Where $y$ denotes experimental data and $f$ represents simulated data in equation (12).

$$R^2 = 1 - \frac{\sum_i (y_i - f_i)^2}{\sum_i (y_i - \bar{y})^2} \qquad \text{(eq. 12)}$$

2.6. Numerical diffusion

While Type1535-1301 greatly reduces the computational effort, the numerical diffusion caused by the simplification may affect the thermal stratification in the water puddle. As shown in Fig. 3, assume that each node in the water zone contains 2 kg of water with a stratification temperature difference of 10 °C. 1 kg/s of hot water enters the puddle from the top. Assuming no conduction and mixing between the nodes, the fluid in the first node will average 70°C over a time step of 2 seconds, while the other nodes will not be affected because there is no conduction or mixing between the nodes. However, the temperature of both the first and second nodes will be affected after 2 seconds at a time step of 1 second. The spurious diffusion of heat is caused by the simplified method of discretizing the geometry into a finite number of nodes; therefore, this is called numerical diffusion.

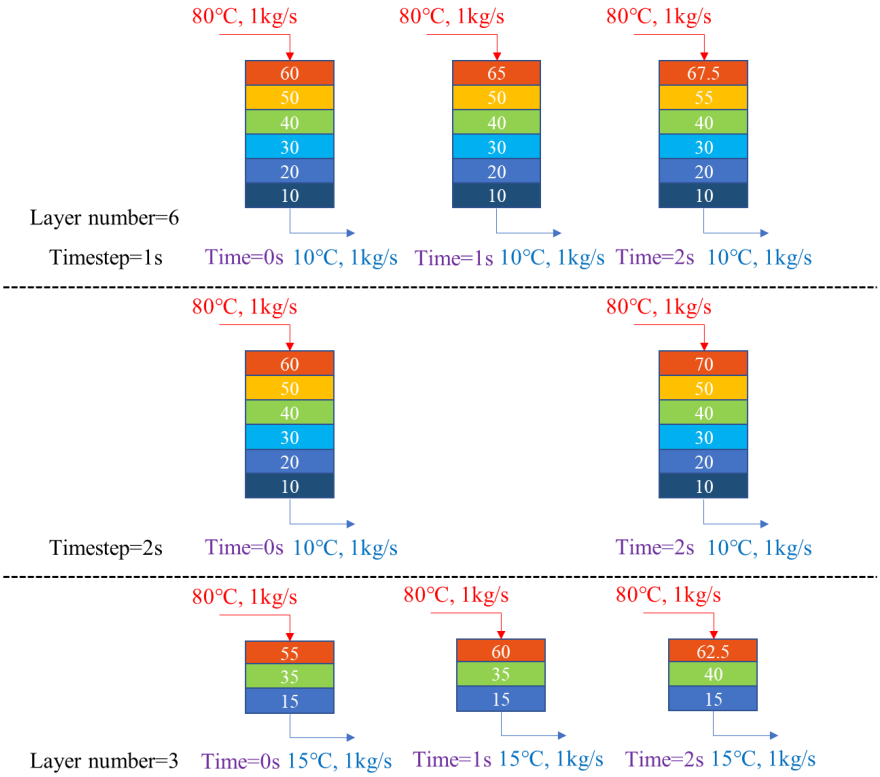


**Fig. 3: Numerical diffusion in the simulation**

It is possible to increase the number of nodes to try to improve the accuracy of the discretization, but this will lead to many computational nodes and longer computational times. And it may numerically extend the effect of node mixing, which in turn is detrimental to the accuracy. The second approach is to set a mixing factor in the model which can determine the volume to be mixed between the nodes. In order to explore the coupling effects of these parameters, the corresponding working conditions settings are given in Table 1.

**Tab. 1: Parameter simulation working condition selection**

| Mixing factor (kg/h) | Timestep (mins) | Nodes number |
|---|---|---|
| adiabatic | 0.5 | 15 |
| 0 | 1 | 20 |
| 1000 | 2 | 32 |
| 10000 | 5 | 50 |
| | 10 | 75 |
| | 30 | 100 |
| | 60 | |

## 3. Results and discussions

### 3.1. The influence of nodes number on thermal stratification

The nodes number (*N*) represent the number of one-dimensional meshes in the PTES, which can be used to study the relationship between meshes and calculation accuracy. Its physical expression can be seen in Fig. 2, which is represented by a symbol (*j*). The selection of nodes number and correlation diffuser location is provided in Table 2.

**Table. 2: Storage discretization and diffuser's location**

| Nodes number *N* | Volume per node ($m^3$) | Top diffuser location | Middle diffuser location | Bottom diffuser location |
|---|---|---|---|---|

| | | | | |
|---|---|---|---|---|
| 15 | 4000 | Node 1 | Node 8 | Node 15 |
| 20 | 3000 | Node 2 | Node 11 | Node 20 |
| 32 | 1875 | Node 3 | Node 17 | Node 32 |
| 50 | 1200 | Node 4 | Node 27 | Node 50 |
| 75 | 800 | Node 5 | Node 40 | Node 75 |
| 100 | 600 | Node 7 | Node 53 | Node 100 |

For the evaluation of thermal stratification, Mix number and stratification coefficients draw different conclusions. Overall in terms of Fig. 4, both indicators reflect that more nodes result in better-calculated stratification. However, this is caused by large nodes ignoring mixing, which is invalid. Mix number agrees better with less than 20 nodes before July, deviates at least with 50 nodes from July to September, is closer to the results with 32 nodes from September to November, and is optimal again with less than 20 nodes after November. The reason for this strange result is the actual mixing at different periods. Although the TRNSYS model cannot calculate the mixing, the larger volume of individual nodes at low node numbers approximates the multilayer mixing. The individual nodes are smaller when the node number is high, thus effectively reducing the numerical diffusion but calculating the mixing worse. New methods are needed to solve this problem, such as setting the mixing coefficient or variable grid treatment. The accuracy of the stratification coefficient is positively correlated with node number because energy moments are not calculated in this formula. The stratification calculation is considered more reasonable as long as the temperature RMS sum is closer to the actual measurement. The Mix number is more realistic if the energy calculation accuracy is taken as a reference. The stratification coefficient is better if the temperature calculation precision serves as the basis.

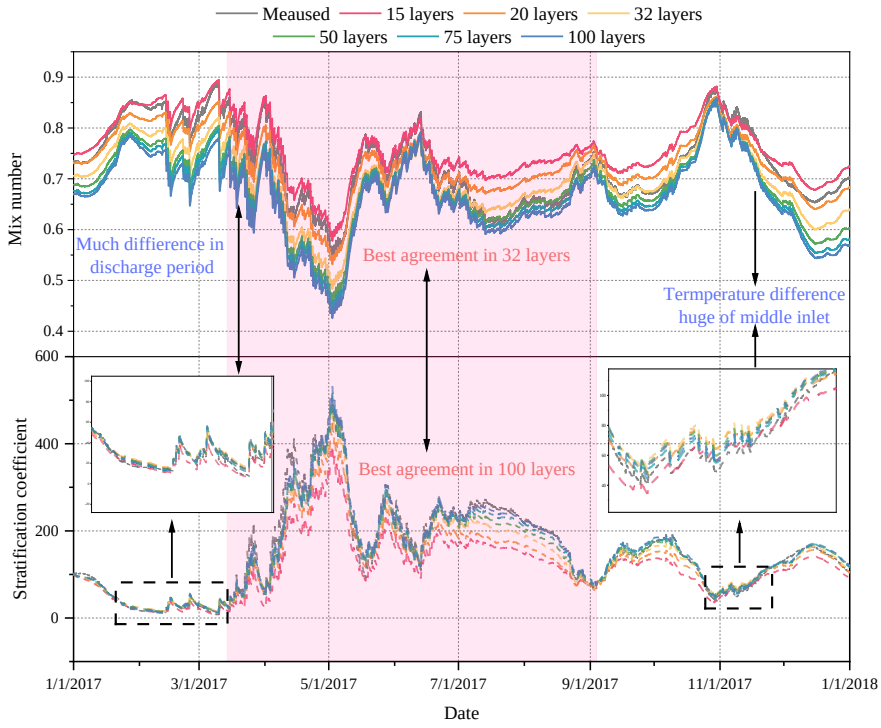


**Fig. 4: Mix number and stratification coefficient changes with nodes number**

3.2. The influence of timestep on thermal stratification

Fig. 5 reflects the effect of different time steps on the stratification calculation. The differences in Mix number and stratification coefficient are very small for time steps below 10mins, indicating that decreasing the time step does not significantly increase the computational accuracy. Therefore, it is undesirable to increase the calculation time by several times to increase the accuracy by less than 0.1%. And when the time step is larger than 30mins, the Mix number has a significantly larger deviation during the energy release. This indicates that too large a time step reduces the computation time at the expense of computational accuracy. Therefore, the time step selection should not be too large either, or 10mins seems to be the optimal choice at 50 node count. The influence law of stratification coefficient and Mix number is basically the same, only the difference will be smaller. It indicates that the temperature dispersion is not as sensitive to the change of time step compared to the energy dispersion.

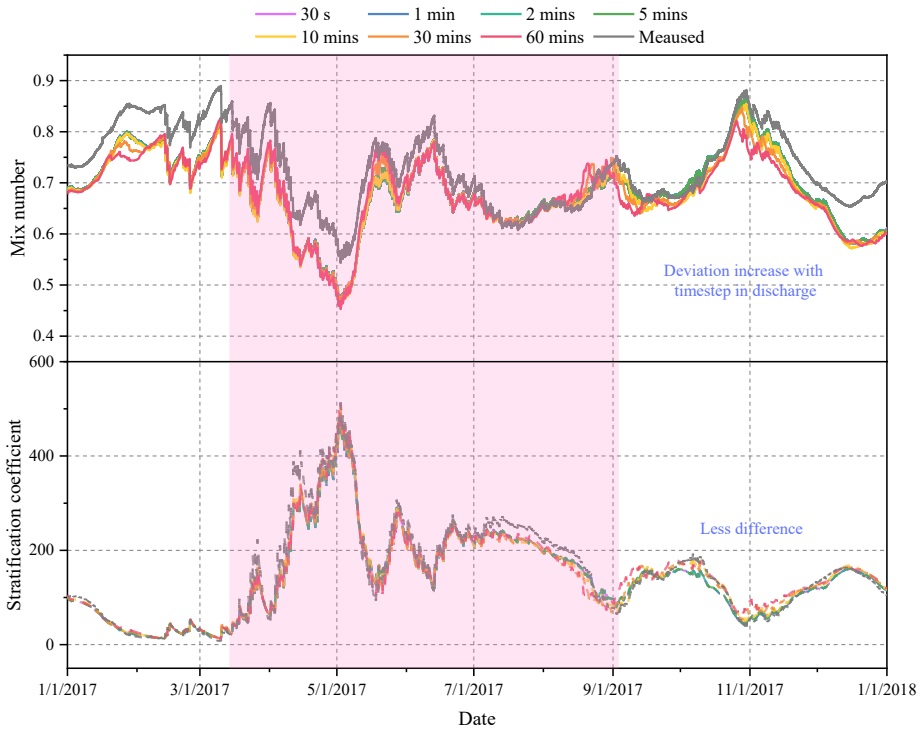


**Fig. 5: Mix number and stratification coefficient changes with timestep**

### 3.3. The influence of Mixing factor on thermal stratification

The treatment of mixing in this model is limited to the energy equation because the momentum equation is neglected. mixing within the PTES is caused by temperature differences and flow rates. Although the heat is eliminated by the assumption of thermal driving force, but it is not consistent with reality. Therefore, the concept of the mixing parameter mmix was introduced to correct this partial deviation. Fig. 6 gives a comparison of four forms of mixing with the actual measurements. 0 kg/h means no mixing, 1000 kg/h means small mixing, 10000 kg/h means large mixing, and finally adiabatic mixing represents node temperature reversal when $j$+1 node temperature is higher than $j$ node temperature. The results show a significant difference between adiabatic mixing and the remaining parameters, especially between April and July during the charging phase. The accuracy of the adiabatic mixing calculation is slightly smaller for all the rest of the time, with the maximum Mix number difference reaching 0.1, implying that 10% of the volume is miscalculated. The exact opposite is true for the stratification factor calculations. The adiabatic blending improves the accuracy of the temperature discretization calculation. Overall, it is demonstrated that adiabatic blending overestimates the degree of dispersion within PTES, which is consistent with the temperature dispersion requirement but not with the energy moment variation.

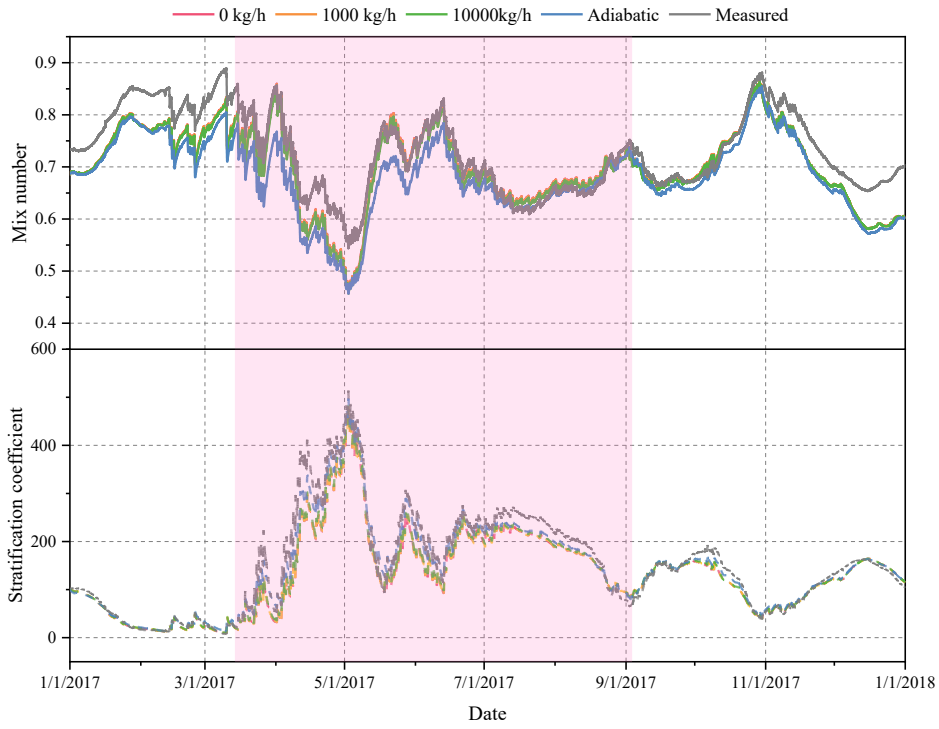


**Fig. 6: Mix number and stratification coefficient changes with Mixing factor**

3.4. Coupling effect of time step and nodes number on calculation accuracy

In the explicit finite difference calculation, the grid size corresponds to a minimum time step as shown in Eq. 13. However, this equation does not specify when the time step is large enough to meet the accuracy requirements with minimal computational resources. This is obviously a serious departure from reality, probably because this formula is only applicable to the refinement of small mesh sizes. Therefore, the mesh size is less meaningful for large size coarse simulations. In this paper, the number of stratifications is used instead of specific dimensions because it is dimensionless. The coupling effect of the number of layers and the time step on the computational accuracy is investigated.

$$min\left\{\frac{1}{\rho c V_k}\sum_j \frac{1}{R t_{kj}}\right\}\Delta\tau \leq 1 \qquad \text{(eq. 13)}$$

The Mix number represents the dispersion of the energy moment inside the PTES and the stratification coefficient represents the dispersion of the temperature inside the PTES. Therefore, only the deviation of the results of these two metrics from the actual measurement needs to be explored to cover all possible maximum deviations. The RMSD and $R^2$ are used to denote the root mean square error and the degree of variation of the stratification number, respectively. Figure 7(a) reflects the accuracy of Mix number calculation, and the results show that 15 nodes work best, with the highest accuracy at 1 min and 60 mins, and the accuracy decreases at 5mins. Conversely, the larger the number of nodes and time step, the worse the accuracy. In particular, at 100 nodes, the coefficient of variation is below 0.1 indicating that less than 10% of the parameters are fully captured and most of the results are not credible. The best matching scheme is 15 nodes with 60mins, 32 nodes with 10mins, 50 nodes with 5mins, and 100 nodes with 1min.

Figure 7(b) reflects the calculation accuracy of the stratification coefficients, and the results show that 100 nodes work best, and the smaller the time step the higher the accuracy. Conversely, the smaller the number of nodes, the worse the accuracy. The coefficient of variation is greater than 0.9 when the number of nodes is greater than 32, indicating that the calculation at this point can capture the experimental results well and with high confidence. 15 nodes have the lowest accuracy for the temperature discretization. The optimal time steps corresponding to each discrete node are 15 nodes with 60mins, 32 nodes with 60mins, 50 nodes with 10mins, and 100 nodes with 1mins.

In summary, it can be concluded that if we pursue computational speed, coarse grid with large time step unexpectedly can achieve good prediction results. This can significantly reduce the computational resource requirements and is suitable for long-term simulations of complex systems at the engineering level. If the highest accuracy is pursued, 32 nodes with 5mins can satisfy the maximum demand of Mix number and stratification factor. However, for the

number of temperature prediction nodes is still the more the better, then a new method is needed to correct the deviation of energy dispersion.

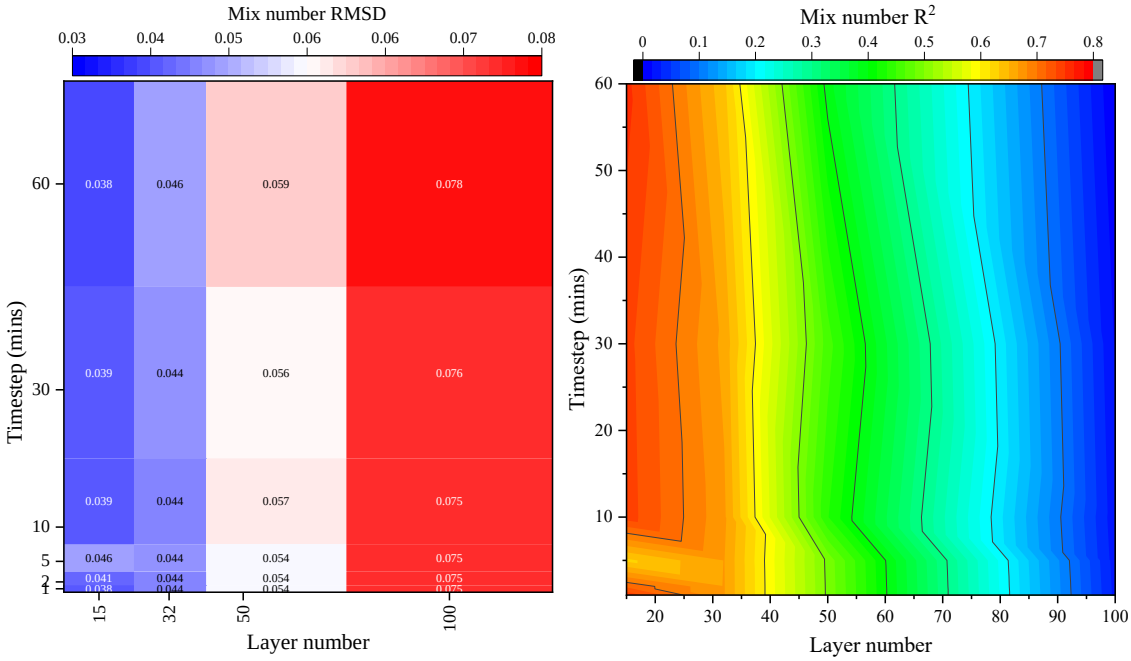


**Fig. 7(a): The coupling effect of time step and nodes number on the Mix number calculation accuracy**

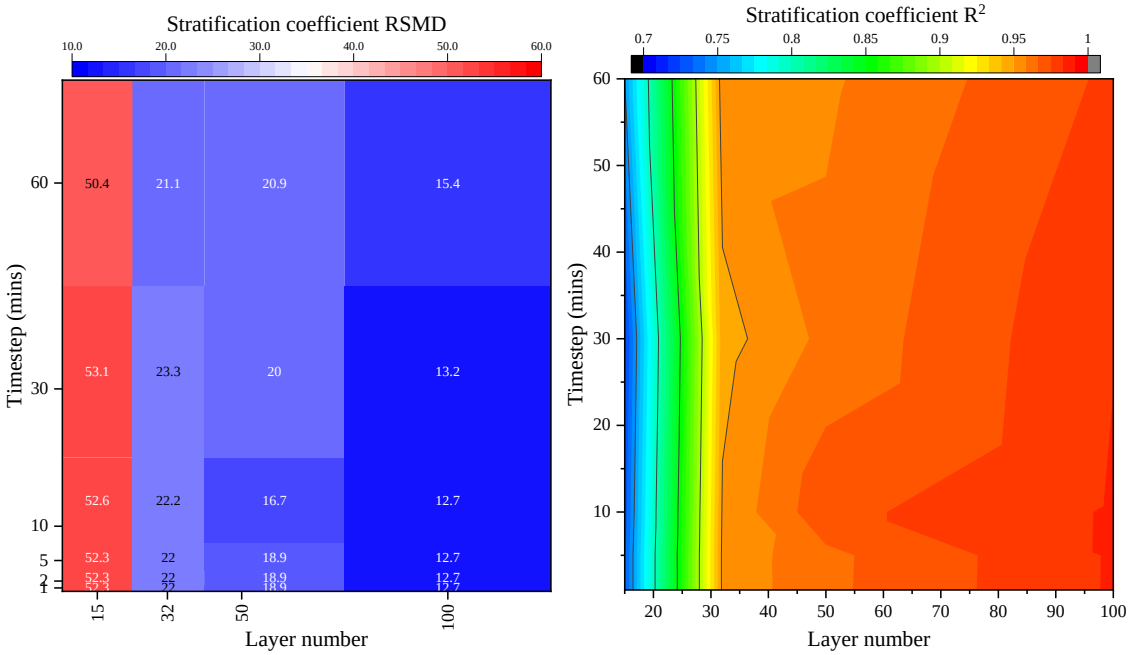


**Fig. 7(b): The coupling effect of time step and nodes number on the stratification coefficient calculation accuracy**

## 4. Conclusions

This paper presents a simulation study of large-scale puddle heat storage by Trnsys and compares it with measured data from a solar district heating plant. The analysis focuses on the computational accuracy of the model for thermal stratification. In addition, the combined effects of the number of nodes, time step and mixing factor on the numerical diffusion are discussed. The following conclusions are obtained.

(1) The number of nodes has the greatest effect on the deviation of the thermal stratification calculation results, with fewer nodes predicting best for energy dispersion and more nodes predicting best for temperature dispersion.

(2) Adiabatic blending and the rest of the mixing coefficients are significantly different, adiabatic blending for energy dispersion prediction is poor, but the prediction of temperature dispersion is better. When the difference between the

results of large blending and no blending is not significant, this indicates that there is not much time for heat transfer by inverse temperature blending.
(3) A small number of nodes is suitable for a long time step and a large number of nodes is suitable for a short time step. 15 nodes with 60mins are most suitable for Mix number prediction and 100 nodes with 1min is most suitable for stratification coefficient prediction.
The accuracy of the calculation of Mix number and stratification coefficients tends to be opposite for different parameters. Therefore, the thermal stratification results of coarse and fine meshes can be considered together when judging the model accuracy or pre-simulation.

## 5. References

Vega Novo, A., Rodríguez Bayón, J., Castro Fresno, D., & Rodríguez Hernández, J., 2010. Review of seasonal heat storage in large basins: water tanks and gravel-water pits. *Appl. Energy*, vol. 87, no. 2, pp. 390–397, doi: 10.1016/j.apenergy.2009.06.033.

Bauer, D., Marx, R., Nußbicker-Lux, J., Ochs, F., Heidemann, W., & Müller-Steinhagen, H., 2010. German central solar heating plants with seasonal heat storage. *Sol. Energy*, vol. 84, no. 4, pp. 612–623, doi: 10.1016/j.solener.2009.05.013.

Bott, C., Dressel, I., & Bayer, P., 2019. State-of-technology review of water-based closed seasonal thermal energy storage systems. *Renew. Sustain. Energy Rev.*, vol. 113, doi: 10.1016/j.rser.2019.06.048.

Heller, A., 1997. Floating lid constructions for pit water storage. A survey.

Egging-Bratseth, R., Kauko, H., Knudsen, B. R., Bakke, S. A., Ettayebi, A., & Haufe, I. R., 2021. Seasonal storage and demand side management in district heating systems with demand uncertainty. *Appl. Energy*, vol. 285, doi: 10.1016/j.apenergy.2020.116392.

Dahash, A., Ochs, F., Janetti, M. B., & Streicher, W., 2019. Advances in seasonal thermal energy storage for solar district heating applications: A critical review on large-scale hot-water tank and pit thermal energy storage systems. *Appl. Energy*, vol. 239, pp. 296–315, doi: 10.1016/j.apenergy.2019.01.189.

Pan, X., Xiang, Y., Gao, M., Fan, J., Furbo, S., Wang, D., & Xu, C., 2022. Long-term thermal performance analysis of a large-scale water pit thermal energy storage. *J. Energy Storage*, vol. 52, p. 105001, doi: 10.1016/J.EST.2022.105001.

Xiang, Y., Gao, M., Furbo, S., Wang, D., Tian, Z., & Fan, J., 2022. Heat transfer of a large-scale water pit heat storage under transient operations. *J. Energy Storage*, vol. 55, p. 105455, doi: 10.1016/J.EST.2022.105455.

Song, M., & Kovacevic, R., 2003. Numerical and experimental study of the heat transfer process in friction stir welding. *Proc. Inst. Mech. Eng. Part B J. Eng. Manuf.*, vol. 217, no. 1, doi: 10.1243/095440503762502297.

Pinel, P., Cruickshank, C. A., Beausoleil-Morrison, I., & Wills, A., 2011. A review of available methods for seasonal storage of solar thermal energy in residential applications. *Renewable and Sustainable Energy Reviews*, vol. 15, no. 7, doi: 10.1016/j.rser.2011.04.013.

Davidson, J. H., Adams, D. A., & Miller, J. A., 1994. A coefficient to characterize mixing in solar water storage tanks. *J. Sol. Energy Eng. Trans. ASME*, vol. 116, no. 2, doi: 10.1115/1.2930504.

Haller, M. Y., Cruickshank, C. A., Streicher, W., Harrison, S. J., Andersen, E., & Furbo, S., 2009. Methods to determine stratification efficiency of thermal energy storage processes–review and theoretical comparison. *Sol. Energy*, vol. 83, no. 10, doi: 10.1016/j.solener.2009.06.019.

Fernandez-Seara, J., Uhı, F. J., & Sieres, J., 2007. Experimental analysis of a domestic electric hot water storage tank. Part II: dynamic mode of operation. *Appl. Therm. Eng.*, vol. 27, no. 1, doi: 10.1016/j.applthermaleng.2006.05.004.

# Appendix

**Nomenclature**

| | | | |
|---|---|---|---|
| $U$ | Heat transfer coefficient, W/(m$^2$·K) | $h$ | Natural convection coefficient, W/(m$^2$·K) |
| $A$ | Area, m$^2$ | $H$ | Height, m |
| $g$ | Gravity, m/s$^2$ | $T$ | Temperature, K |
| $D$ | Diameter, m | $V$ | Volume, m$^3$ |
| $C_p$ | Specific heat of water, J/(kg·K) | $c$ | Specific heat of soil, J/(kg·K) |
| $r$ | Distance in radial direction, m | $m$ | Mass quality of each tank node, kg |
| $Q$ | Energy, J | $z$ | Distance in vertical direction, m |
| $M$ | Energy Moment, J·m | $n$ | 1-D simulation PTES nodes |
| $ST$ | Stratification number | $MIX$ | Mix number |

*Subscripts*

| | | | |
|---|---|---|---|
| mea | Measurement | sim | Simulation |
| w | Water | HDPE | HDPE-liner |
| geo | Geotextile | side | Side of the storage |
| bot | Bottom of the storage | top | Top of the storage |
| $j$ | Elements in 1D region | $i,k$ | Elements in 2D region |
| loss | Heat loss | in | Inlet |
| s | Soil | ins | Insulation |
| ch | Charging | dis | Discharging |
| mix | Mixing | t | Total |
| thermo | Thermocline | str | Stratification |
| cold | Inlet water in minimum temperature | hot | Inlet water in maximum temperature |
| far | Far-field of soil | c | current |
| deep | Deep of soil | | |

*Greek*

| | | | |
|---|---|---|---|
| $\rho$ | Density, kg/m$^3$ | $\lambda$ | Thermal conductivity, W/(m·K) |
| $\Delta$ | Difference | $\tau$ | Time, s |
| $\theta$ | Slope angle, ° | | |